Improved fabrication of zero-mode waveguides for single-molecule detection

Mathieu Foquet,[a] Kevan T. Samiee, Xiangxu Kong, Bidhan P. Chauduri, Paul M. Lundquist, Stephen W. Turner, Jake Freudenthal, and Daniel B. Roitman
Pacific Biosciences, 1505 Adams Drive, California 94025, USA

(Received 13 September 2007; accepted 12 November 2007; published online 4 February 2008)

Metallic subwavelength apertures can be used in epi-illumination fluorescence to achieve focal volume confinement. Because of the near field components inherent to small metallic structures, observation volumes are formed that are much smaller than the conventional diffraction limited volume attainable by high numerical aperture far field optics (*circa* a femtoliter). Observation volumes in the range of 10^{-4} fl have been reported previously. Such apertures can be used for single-molecule detection at relatively high concentrations (up to 20 μM) of fluorophores. Here, we present a novel fabrication of metallic subwavelength apertures in the visible range. Using a new electron beam lithography process, uniform arrays of such apertures can be manufactured efficiently in large numbers with diameters in the range of 60–100 nm. The apertures were characterized by scanning electron microscopy, optical microscopy, focused ion beam cross sections/transmission electron microscopy, and fluorescence correlation spectroscopy measurements, which confirmed their geometry and optical confinement. Process throughput can be further increased using deep ultraviolet photolithography to replace electron beam lithography. This enables the production of aperture arrays in a high volume manufacturing environment. © *2008 American Institute of Physics*. [DOI: 10.1063/1.2831366]

INTRODUCTION

Single-molecule studies probe in detail the finer aspects of molecular biology,[1–4] including distributions around the ensemble average, detailed molecular dynamics, and kinetic parameters and anomalous diffusion. Many techniques for achieving single-molecule detection have been devised, ranging from confocal detection,[5] stimulated emission depletion[6] (STED), optical trapping,[7] confined microfluidics structures,[8–13] immobilization in a solid matrix,[14,15] to near field probes.[16–22] These approaches are driven by a need to obtain optical confinement to observe single fluorophores at relatively high background concentrations.

Near field techniques are an especially powerful means to achieve the type of high optical confinement that can be applied to study molecular biology problems using fluorescence probes at biologically relevant concentration. Structures such as gold tips,[17,23] near field tips,[24,25] total internal reflectance fluorescence (TIRF) microscopy,[26,27] or evanescent wave structures[28,29] have all been used to excite and detect single-molecule fluorescence. One of the most promising structures so far to have achieved single-molecule detection is the zero-mode waveguide (ZMW, see Fig. 1).[16,30–32]

The conceptually simple ZMW structure, shown in Fig. 1, creates a small observation volume and allows observation of single fluorophore diffusion,[16] reaction equilibrium and kinetics,[30] or membrane diffusion.[31] When used in epi-illumination [Fig. 1(b)], in combination with conventional fluorescence dichroic, filters, and imaging optics, a very small illuminated volume is formed at the bottom of the structures [Fig. 1(c)].

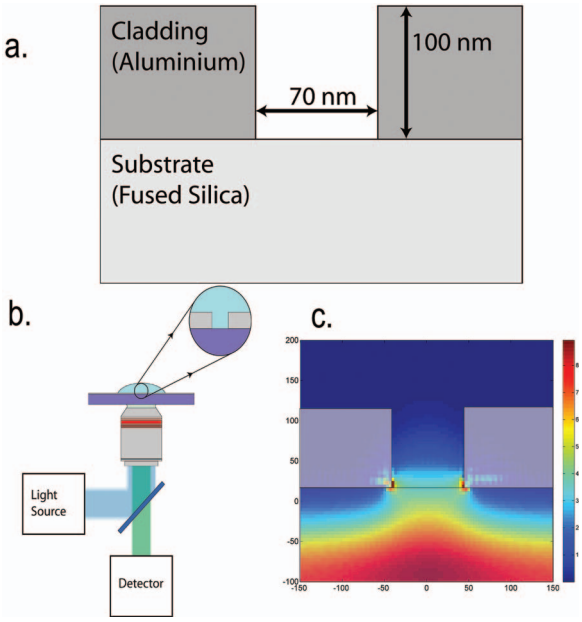

FIG. 1. (Color) Zero-mode waveguide schematics and fluorescence excitation. (a) Illustration of a single ZMW made with aluminium as a cladding material and fused silica as a substrate. (b) Schematic of usage of ZMWs for fluorescence excitation. In epi-illumination, a light source is used to shine light on the metal-glass interface of the ZMW. Fluorophores present in the observation volume created by this excitation light will be excited and will emit fluorescence that can be recollected using the same microscope objective used for excitation. Dichroic optics and additional filters can be used to separate the excitation from the emission light. (c) The insert shows how the subwavelength apertures constrain light to only the lower section of the ZMW, creating a small excitation volume.

[a]Electronic mail: mfoquet@pacificbiosciences.com.

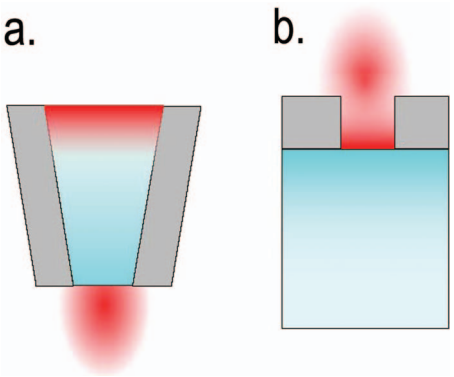

FIG. 2. (Color) Near field aperture and zero-mode waveguide. In an NSOM tip (illustration a), the field is exponentially attenuated within the metal clad tip. As it exits the tip, the field expands quickly, approximately following some rational law with distance from the tip. It is this polynomial field that is used to excite fluorescence in NSOM applications. It is also worth noting that, due to losses in the tip, the field outside the tip is much weaker than the field existing in the tip. Conversely, in a ZMW (illustration b), it is the exponential field existing in the metal clad area that is used for fluorescence excitation; while the rational field outside the ZMW is unused.

ZMWs provide stronger confinement than the more conventional near field scanning optical microscopy (NSOM) tips.[19,33] Although the two geometries are reminiscent of each other (see Fig. 2), they rely on different physical mechanisms. In an NSOM tip, it is the field existing outside the metal clad tip that is used to excite fluorescence, this field intensity decays approximately as an inverse power of the distance from the tip. The zero-mode waveguide takes advantage of the exponentially decaying field existing inside the metal clad waveguide at cutoff. Because of the functional difference in the spatial dependence (polynomial to exponential) of the light intensity, the ZMW provides stronger confinement and better performance when used for single-molecule detection at high concentration. Furthermore, ZMWs can be mass manufactured and used in parallel detection systems.

Previous publications[16,34] have outlined ZMW fabrication processes based on directly etching or ion milling the openings into the metal. Here, we present a new method of manufacturing dense arrays of ZMW in large quantities using a negative tone, single exel, metallization, shear removal (NEMS) process. This new process yields reliable, uniform structures when implemented in a controlled environment. The NEMS process uses negative tone patterning in which pillars of resist are first defined on the surface of the substrate and then metal is evaporated around these pillars. The structures are then freed using a combination of solvent and sonication to remove the excess metal from the top and sides of the pillars. This process was used to fabricate ZMWs. The manufactured structures were thoroughly characterized using a combination of methods. Scanning electron microscopy (SEM) and focused ion beam/transmission electron microscopy (FIB/TEM) measurements confirmed the physical dimensions and integrity of the structures manufactured. Optical microscopy was used as a high-throughput method to measure variability either within the ZMW array or between fabricated samples. Finally, fluorescence correlation spectroscopy (FCS) confirmed that the structures behave according to previous literature[16] when used in the context of single-molecule fluorescence detection. The benefits of the NEMS process are severalfold, including, for example, increased feature uniformity compared with less reproducible metal etching processes, while maintaining fabrication throughput. Further, by adopting slight modifications, such as the use of a deep ultraviolet (DUV) photolithography stepper, the NEMS process is shown to be highly scalable so readily transferred to true high volume manufacturing (HVM) processes.

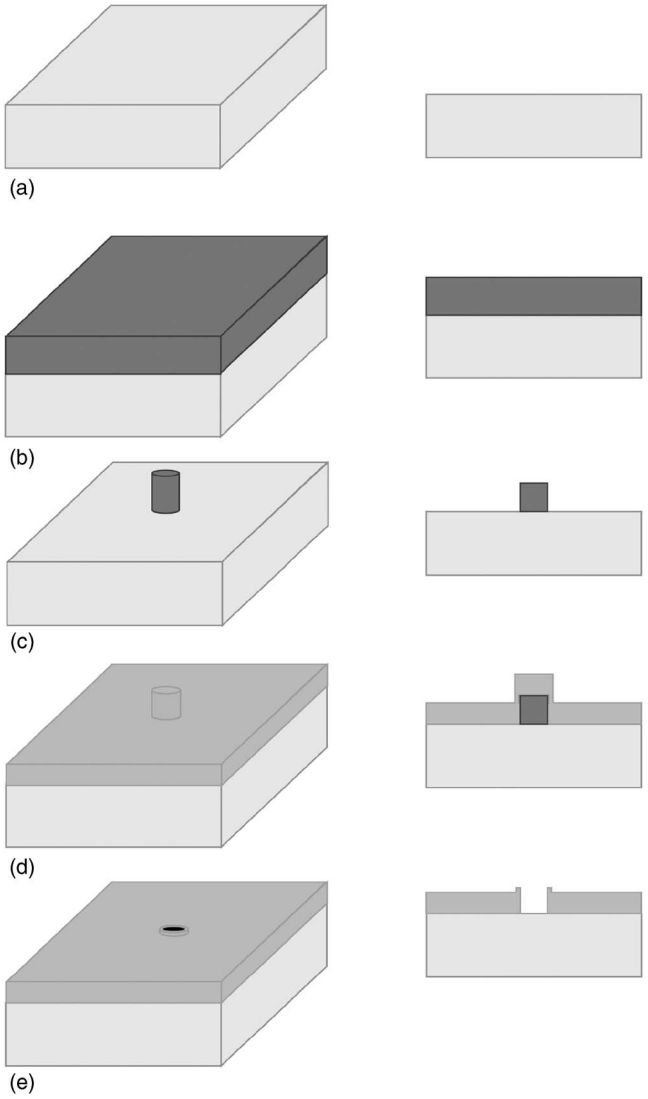

FIG. 3. A Schematic of the fabrication of zero-mode waveguides using a negative tone process. (Step a) The substrates are cleaned and prepared for patterning. (Step b) A negative electron beam resist is coated onto the wafer and baked. (Step c) Exposure and development of pillars. (Step d) Aluminium deposition on the pillar. (Step e). Lift-off and formation of the ZMW.

METHODS

Electron beam lithography

The fabrication (presented schematically in Fig. 3) can be broken down in five principal steps. These are cleaning, pre-exposure coatings, exposure, metallization, and opening. These are shown, respectively, as steps a–e in Fig. 3.

Fabrication of the ZMW arrays was carried out using 100 mm diameter, 175 ± 13 μm thickness wafers made from Corning 7980 fused silica as the underlying substrate. The wafers were cleaned using a SC-1 bath (ammonium hydroxide, hydrogen peroxide, and water in 1:1:5 v/v ratio) heated to 75 °C. The wafers were immersed for 10 min in the bubbling bath to remove contamination from organics and other contaminants. After 10 min, the wafers were rinsed in a de-ionized water cascade bath until resistivity reaches 16 MΩ cm, The wafers were then spun dry in a spin rinse dry (SRD) system (STI, Kalispell, Montana, USA).

Further cleaning in an oxygen plasma was performed. The wafers were placed in a Branson barrel etcher for 10 min and subjected to 1000 W oxygen plasma under 1.25 Torr of pressure and an oxygen flow of 125 SCCM (SCCM denotes cubic centimeter per minute at STP). This step removes remaining moisture from the surface. Following plasma cleaning, the surface was primed for resist adhesion using hexamethyldisilazane. The standard process of a YES-LPIII oven (Yield Engineering System, Livermore, California, USA) was used for priming. After priming, a 300 nm layer of NEB-31A negative electron beam lithography resist (Sumitomo Chemical America, New York, New York, USA) was spun on the wafer keeping spin speed at 4 500 rpm for 60 s. Following application, the resist was baked for 2 min at 115 °C on a hot plate.

Wafer and resist were coated with a thin layer of gold so as to provide a charge dissipation path during exposure on the electron beam lithography tool. This was accomplished by using physical vapor deposition to apply a 10 nm layer of gold on top of the NEB-31 resist.

A Leica VB-6 UHR system (Vistec, Weilburg, Germany) was used for the feature patterning step. The ZMWs were exposed as single, 5×5 nm^2 (corresponding to a 328.67 μm field size and a 14 bit digital-to-analog converter) exposure elements (exels). Doses ranged from 10 000 to 120 000 μC/cm^2. Before the development occurred, the resist was baked on a hotplate at 90 °C for 2 min. The gold overcoat was removed in Transene gold etch TFA (Transene, Danvers, MA, USA). For this, the wafers were immersed in the gold etchant for approximately 10 s and rinsed with de-ionized water. The wafer at this stage was ready for development in MF-321 developer (Shipley, Marlborough, MA, USA). The wafer is immersed for 30 s in the developer then thoroughly rinsed and dried. Since NEB-31 is a negative resist, this exposure pattern leaves arrays of pillars on the surface of the wafer after the development, as can be seen in Fig. 4(a).

A short descum step was applied next to the wafer to prepare the surface for aluminium coating using a Glenn 1000 plasma asher (Yield Engineering Systems, Livermore, CA, USA) under the following conditions: 100 W forward power, 18 SCCM oxygen, and 125 mTorr for a duration of 45 s. The aluminium was evaporated thermally on the developed wafer in a SC-4500 evaporator (CHA Industries, Fremont, CA, USA) using a tungsten boat (PVD Materials, Wayne, NJ, USA). The deposition rate was kept around 2.5 nm per second and the thickness is monitored, *in situ*, using an Inficon XTC-3 deposition controller (Inficon, Syracuse, New-York, USA). Following deposition, the actual thickness was checked using a P-10 Tencor profilometer (KLA-Tencor, San Jose, CA, USA). Nominal thickness of the metallic layer is 110 nm; thicknesses in the range of 30–170 nm were also deposited to investigate the limits of the process.

The structures were then finished by removing the metal caps. For this, the wafer is entirely immersed in Microposit 1165 photoresist stripper (Shipley, Marlborough, MA, USA) and placed in a sonication bath (Branson, Danbury, CT, USA) for approximately 5 min. Under sonication, the aluminium heads at the top of the resist pillars break off and the resist pillars are dissolved away, leaving behind the imprint of the pillars [Fig. 4(c)].

Photolithography

In this approach, most of the process remains identical and only the patterning steps are modified (steps b and c in Fig. 3). The wafers were cleaned as described before. They are then coated with 80 nm of an antireflection coating, Brewer 29-A Barc (Brewer Sciences, Rola, MO, USA) and 280 nm of Rohm-Haas Epic V41-0.28 positive resist (Rohm-Haas, Philadelphia, PA, USA).

The wafer was coated, exposed, and developed on a fully integrated modern DUV stepper, an ASML 550/9xx 193 DUV production stepper (ASML, Veldhoven, Netherlands). The antireflection coating was removed postdevelopment in an oxygen plasma. At this point, the wafer was treated in the same manner as in the electron beam lithography process and standard metallization and resist pillar removal steps were executed as described in the electron beam lithography process.

Sample preparation

After fabrication, the wafers were diced into individual 6×6 mm^2 square chips. Alignment of the pattern with the dicing tool was done through a set of larger features patterned using the lithography tool and placed along the edges of the wafer. This allowed for accurate dicing of the wafer. The chips were then mounted to special microscope slides into which a 3 mm diameter hole was made, using Norland 81 glue (Norland Optical Adhesives, Cranbury, NJ, USA) as an adhesive. A plasma clean was performed to prepare the surface under a pressure of 2 Torr and 500 SCCM of oxygen flow using a Harrick Plasma Cleaner (Harrick Plasma, Ithaca, NY, USA).

For FCS, the fluorescent samples were prepared by diluting the required dye, Alexa488 (Invitrogen, Carlsbad, California, USA) to a working concentration of 10 μM in 50 mM MOPS-acetate buffer with 75 mM potassium acetate, 20 mM ammonium acetate, and 5 mM dithiothreitol. A 8 μl of the dye solution was then loaded in the reaction well and the sample was measured.

Instrumentation

For optical microscopy inspection, an inverted IX-71 (Olympus, Tokyo, Japan) microscope fitted with an automated stage (Prior Scientific, Rockland, MA, USA) and a black and white charge coupled device (CCD) camera Cool-

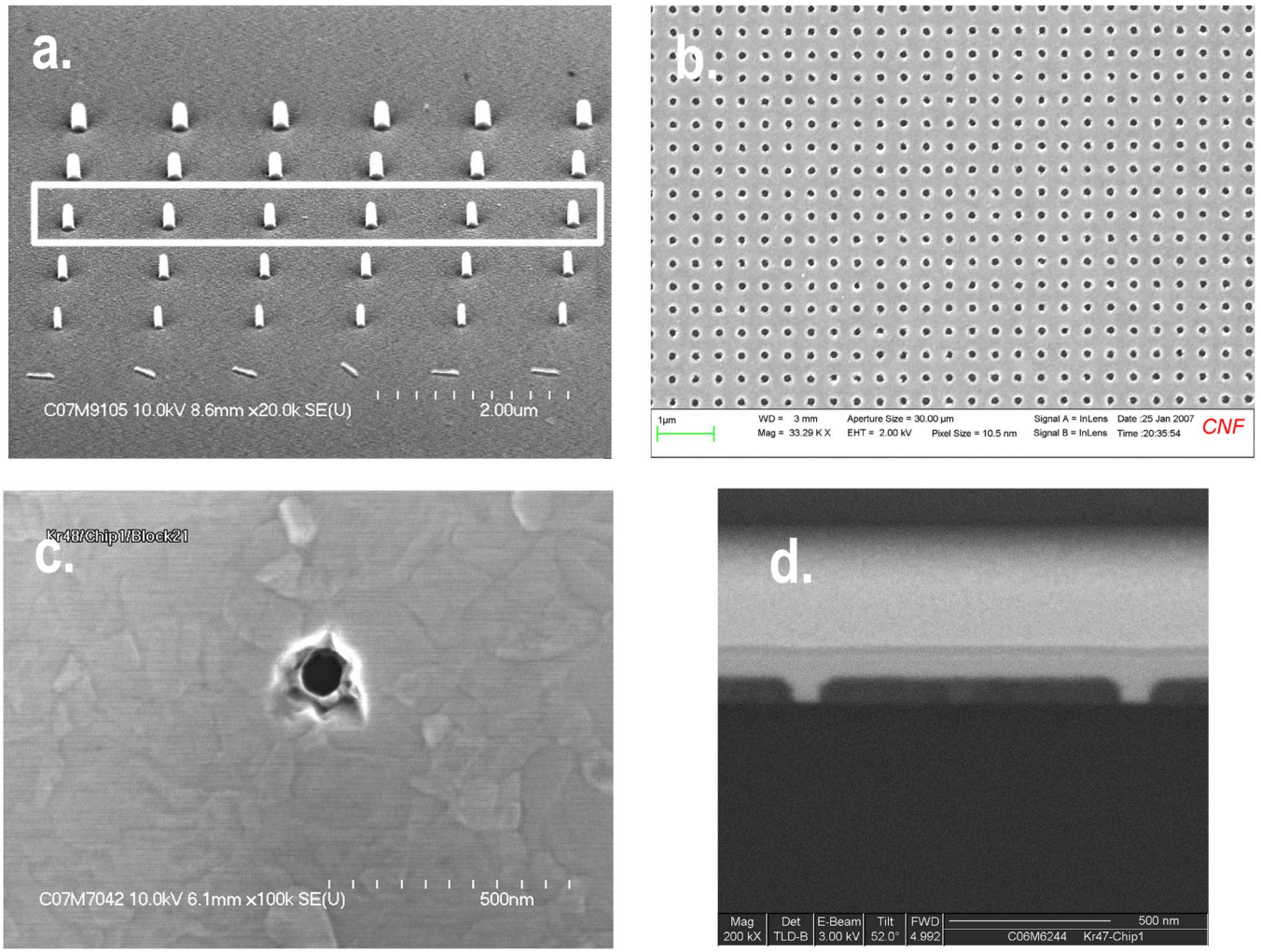

FIG. 4. (Color online) Images of fabricated zero-mode waveguides. (a) A scanning electron microscope picture of the resist pillars after development. The sample was coated with 10 nm of a gold/palladium alloy for the purpose of electron microscopy imaging. The size of the smallest pillars still standing is 40 nm while the largest are around 110 nm in diameter. The target CD of 70 nm is indicated by the white box around the third row from the top. (b) A scanning electron microscope image of an array of ZMWs showing good uniformity. ZMWs are arrayed at a pitch slightly above the Abbe resolution limit for a high numerical aperture microscope objective. At this density, approximately 6.25 million ZMWs can be placed in an area of one square millimeter. (c) Top down view of a ZMW formed by the negative tone process. (d) Cross section formed by a dual beam FIB system. The sidewalls are straight at the base and show some rounding around the top of the structure.

snap ES (Photometrics, Tucson, AZ, USA) was used to collect images of the manufactured chip. The images were first analyzed using a segmentation algorithm to identify all the ZMWs. The segmentation algorithm also takes advantage of the ZMWs grid layout to both exclude parasitic signal and perform background correction. Once the ZMW are located, statistical analysis is performed on the groups of pixels associated with each individual ZMW.

For fluorescence correlation spectroscopy, a separate inverted IX-71 microscope was used as the platform for the experiment. An argon-ion laser (Melles Griot, Carlsbad, CA, USA) is used to excite the fluorescence at 488 nm. The laser beam is expanded to fill the back aperture of the objective used, a 60×, water immersion, 1.2 numerical aperture (NA) microscope objective (Olympus, Tokyo, Japan). A side port is adapted to accept two 50 μm core, step-index fibers (OZ Optics, Ontario, Canada). The light from the ZMW is split equally between the two fibers and directed toward identical single-photon avalanche photodiodes (SPCM-AQR-14-FC, PerkinElmer, Fremont, CA, USA). A universal serial bus (USB) correlator unit (Flex01LQ-5, Correlator.com, Bridgewater, NJ, USA) is used for the analysis of the signal from the photon counting module and calculation of the correlogram.

RESULTS

Fabrication

ZMWs with diameter in the range of 40–150 nm are readily manufactured in 100 nm thick metal films. At the lower end of the diameter range, the resist pillars were found to adhere to the substrate during the drying step following development. At the high end, the pillar sidewalls no longer exhibit a sufficiently vertical profile, leading to difficulties in the lift-off step. The process was also found to be usable over a reasonable range of metal thicknesses. There was no lower limit for how thin a metal film can be made, and the process yields acceptable results with metal thicknesses up to

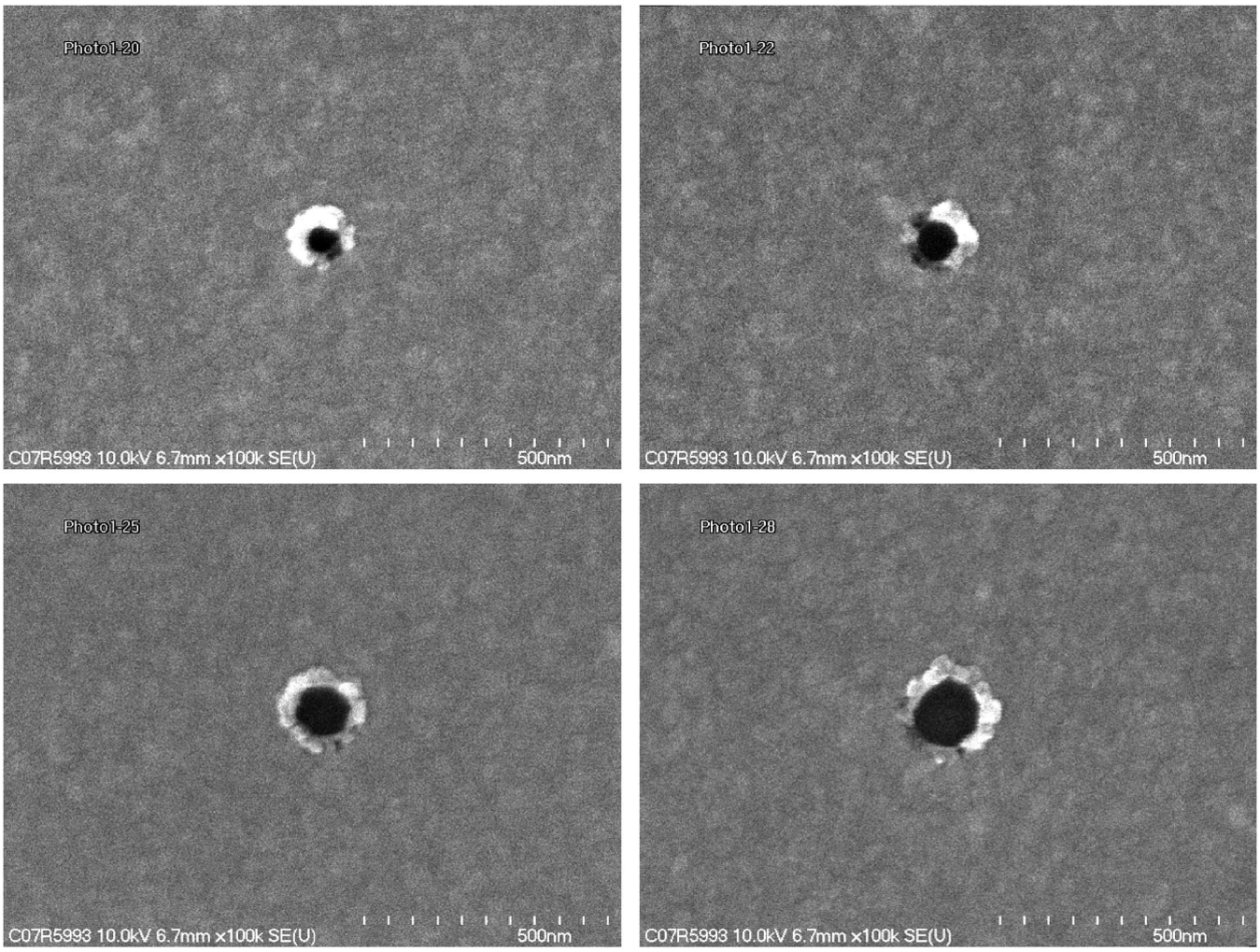

FIG. 5. Images of zero-mode waveguides fabricated by DUV photolithography Pictures of four ZMWs, with sizes ranging from 50 to 100 nm manufactured by the photolithography based CV process. This confirms that the process can be extended to a photolithography based process, thus allowing high volume manufacturing of ZMW chips.

170 nm and diameters of 50–110 nm. At higher thicknesses, lift-off difficulties decrease the yield of usable ZMWs. Although thicker films provide better rejection of the background fluorescence component generated by the bulk of the solution, it was found that 100 nm provides sufficient signal to noise ratio to perform adequate single-molecule detection, while maintaining a very high yield in the manufactured structures.

The NEMS process can be used to readily manufacture large arrays of regular ZMWs. Uniform arrays with inter-ZMW spacing ranging from 300 nm to several micrometers were manufactured [400 nm pitch shown in Fig. 4(b)]. The arrays' uniformity was demonstrated through extensive SEM characterization and was confirmed by an analysis of the optical properties of the fabricated structure. The two data sets provide solid evidence of the quality of the arrays of ZMWs manufactured using the NEMS process. The cross section of the ZMW shows some degree of tapering near the entrance [Fig. 4(d)]. The tapering is attributed to shadowing effect from the pillar during the metallization step, and had little impact on the performance of the ZMW arrays in optical confinement.

Multiple features of the fabrication process provide advantages. First, the relatively low density of features in the pattern means that no proximity corrections are required. The single exel approach enables the use of dose as a direct control for the size of the finished structures. Good uniformity and dimensional control of the process are obtained by avoiding the difficulties inherent in a metal etch step where the native oxide acts as an undesired source of variability in the absence of a hard etch mask. Second, another advantage of a negative tone process is the simplicity of changing the metal cladding of the waveguide. Any metal that can be deposited using a PVD process can now be used for forming ZMWs. This circumvents the need to develop alternate etch chemistries, something that can prove to be a major technical hurdle, as not all metals have available etch recipes.

Finally, The high throughput of the method is a direct result of the fact that the fill fraction of the written pattern is less than $2.5\times10^{-3}\%$ while the fill fraction of the finished product is approximately 0.25%. At such low fill fractions, the electron beam patterning is fast, thereby circumventing the usual limit of electron beam lithography. An entire array of approximately 100 000 ZMWs, covering an area of ap-

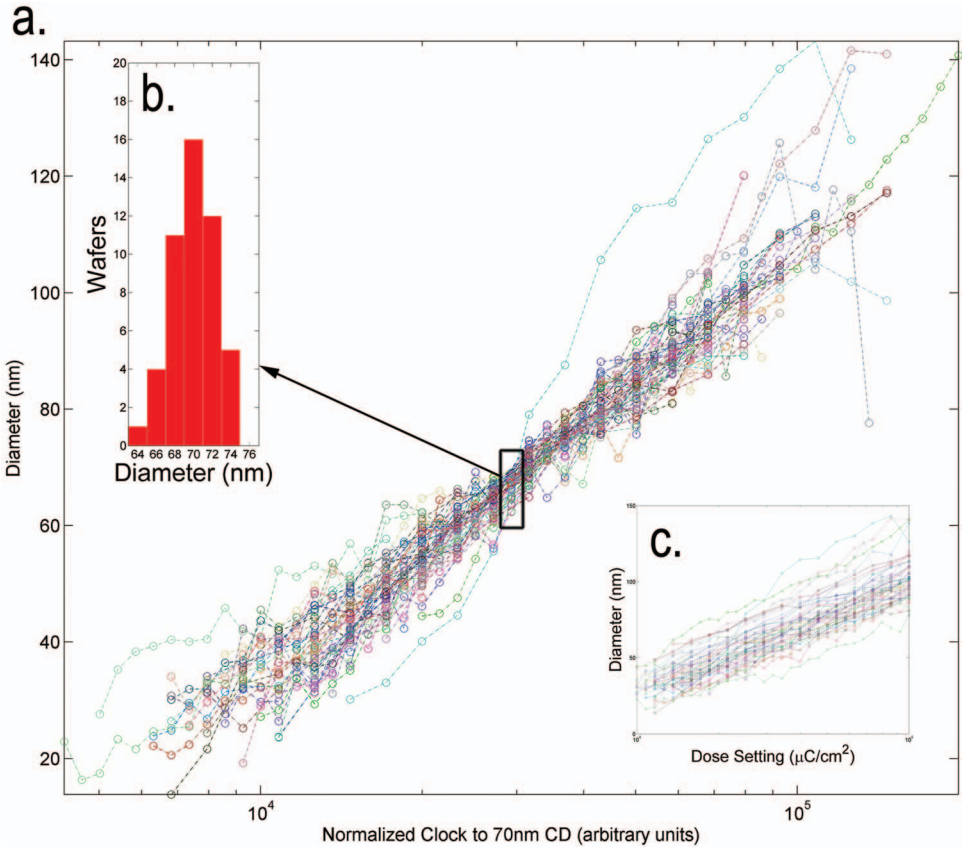

FIG. 6. (Color) Diameter control by scanning electron microscopy. (a) Plot of distribution of diameters on single chips. The electron beam dose axis has been normalized so that the 70 nm diameter feature falls at the same position, compensating to the variability of the process due to manual postexposure baking and developing. (b) Distribution of 70 nm diameter features (all points from graph a falling inside the marked box) as selected from the existing population of ZMW sizes present on 40 wafers. Average is 70 nm and standard deviation is 2.5 nm. (c) Raw data from the 40 wafers used in the previous data. Plot of the diameter as a function of direct dose on the electron beam lithography process.

proximately 1 mm^2 forming a unit die, can be exposed in under 18 s and a wafer including approximately 150 such arrays in under an hour with much of that time consumed by the 14 stage moves necessary to span the 1.2×0.9 mm^2 rectangle that encompasses the array. The fourteen stage moves are required since the electron beam lithography tool has a field size of only 300 μm^2. Optimization of the array design, or use of an electron beam lithography system with larger field sizes should significantly lower exposure time.

While this article focuses on the fabrication and characterization of ZMWs using the electron beam lithography process steps, higher throughput was demonstrated through the use of a modern DUV stepper. Because the pitch of the ZMWs (300 nm and up) is much larger than their diameter, small features can easily be obtained by overexposing slightly the resist with a binary mask. This is in contrast with conventional complementary metal oxide semiconductor (CMOS) electronics where the linewidth requirement, com-

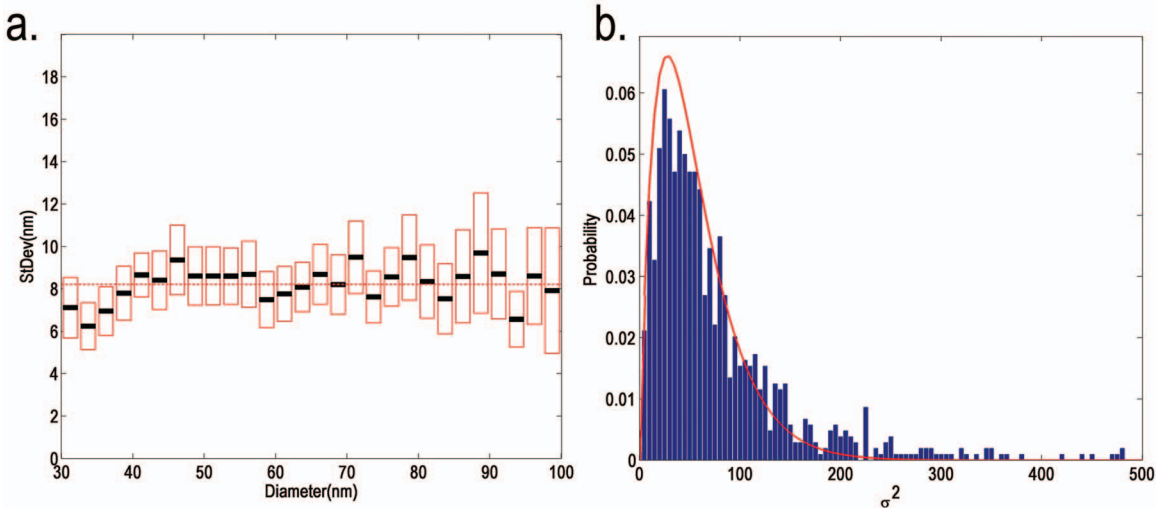

FIG. 7. (Color) Dimensional control of the fabrication technique. (a) Standard deviation (black mark) of ZMW diameter and measured error (red box) plotted as a function of the ZMW diameter. Data are for the same wafers that were used in Fig. 6. The dashed red line is the average of the entire data set. (b) Histogram of distribution of σ^2 (blue) for the data set. The red line is a χ^2 distribution with four degrees of freedom corresponding to the theoretical distribution associated with the five measurements per chip performed.

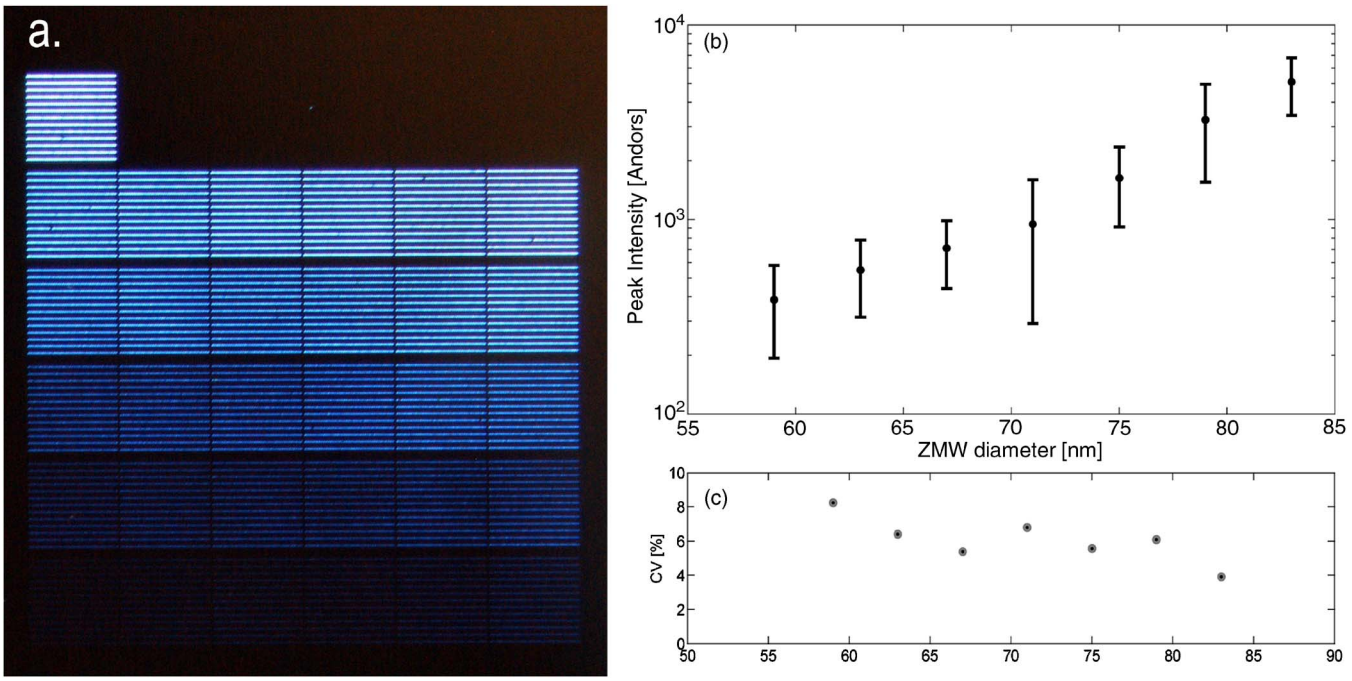

FIG. 8. (Color online) Image of zero-mode waveguide and transmitted light quantification. (a) Picture of Arrays of ZMW. Each square in the above picture is made of an array of 13 lines of 39 ZMW each. As we move down the array, the dose of the electron beam system was decreased, leading to the formation of smaller and smaller ZMW. At sufficiently high magnification, the individual ZMW can be identified and the amount of light can be quantified. (b) Plot of the logarithm of transmission through the individual waveguides as quantified from the optical microscopy pictures as a function of dose number. The plot shows that waveguides within a single dose are uniform as seen in transmission. (c) Plot of corresponding coefficient of variation. Trending and value range of the coefficient of variation are similar as that found for the SEM data, thereby confirming the quality of the structures formed by the new CV manufacturing process.

bined with the pitch, forces extensive use of proximity correction and gray-level mask technology. The use of a DUV stepper boosts the throughput to an even higher level with patterning of up to 120 wafers an hour, for a total maximum of approximately 20 000 chips per hour. The ZMWs manufactured by this process show similar features to those manufactured by the electron beam lithography process (Fig. 5). Optimization of focus and exposure setting will allow for a finer control of ZMW profile than what the dose control on the electron beam lithography allows. This modification to the process enables mass manufacturing of ZMWs arrays.

Electron microscopy

Extensive characterization of the structures was conducted by SEM. For each wafer manufactured, two dice are selected for imaging. For each dose setting on the electron beam lithography tool, five pictures of ZMWs are taken from each die, as shown in Fig. 4(c). The diameter of the corresponding structures is determined through a segmentation algorithm[35] that effectively measures the area in the picture associated with the low secondary electron yielding opening in the metal film.

The 10 pictures per dose are averaged together, and ZMW size can then be plotted as a function of electron beam dosage [Fig. 6(c)]. Most of the resulting wafer-to-wafer variability stems from the manual steps of the post exposure bake and development. To compensate for this handling induced variability, a normalized dosage can be computed by resetting the dose for which ZMW diameter is closest to 70 nm to the nominal dose of 15 000 $\mu C/cm^2$. All other doses are then normalized by the corresponding multiplicative factor [Fig. 6(a)].

In the range of dosage, the diameter exhibits used a linear dependency on the logarithm of the dose. This is approximately expected, from the combination of a Gaussian beam tool used for exposure, with the response curves from a chemically amplified resists.[36] The distribution of sizes around the nominal diameter of 70 nm is dominated by the slope of the diameter/dose curve. This slope is relatively independent of the manual components of the process [Fig. 6(a)] allowing targeting of the nominal diameter to within 2 nm [Fig. 6(b)].

Finally, the variability of the ZMW size within each chip was determined by computing the standard deviation σ of ZMW diameter as estimated from the two groups of five pictures taken at each electron beam dosage. The process yields a ZMW to ZMW variability of around 8 nm that is relatively independent of the critical dimension (CD) [Fig. 7(a)]. The distribution of σ^2 around its average value follows closely the theoretical χ_4^2 distribution, indicating that the dominant term in the distribution of σ^2 is the measurement error due to the sampling of five pictures.

Transmitted light analysis

We developed a higher-throughput method to analyze the variability in ZMW structures using light transmittance. The amount of light able to pass through the structure when it is illuminated was quantified and allows a comparison of

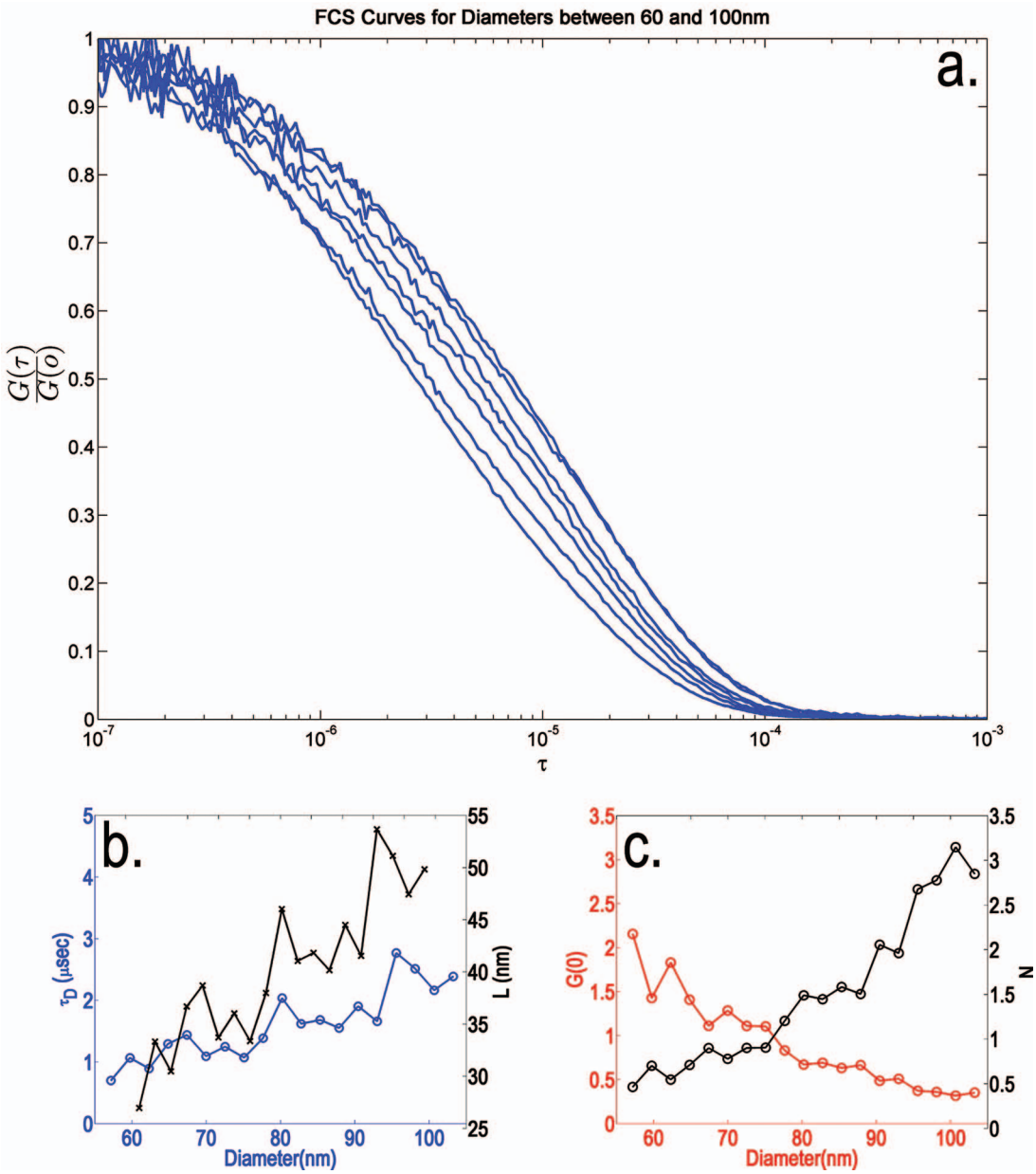

FIG. 9. (Color) Diffusion time as a function of diameter. (a) FCS curves of ZMW of different diameters, ranging from 56 (leftmost curve) to 104 nm (rightmost curve) by steps of approximately 8 nm). The autocorrelation function has been normalized to show more clearly the change in residence time that is cause by the diameter change. (b) Diffusion time as a function of ZMW diameter and calculated decay length in the ZMW based on the diffusion time. (c) $G(0)$ and number of molecules present in the focal volume as a function of diameter of the ZMW.

the optical properties of nominally identical ZMWs. Figure 8(a) shows a typical picture of an array of ZMW. For transmitted light analysis, similar pictures were taken with a black and white camera and the sum intensity of all the pixels associated with a single ZMW was calculated and then corrected for the background.

Figure 8(b) shows the raw results of such quantification. Since transmitted light is well approximated by a log-linear function of diameter for subwavelength apertures in this regime,[37–40] this information serves as an indirect measure of the relative diameter of each individual ZMW. Since the electron beam exposure process is also log linear in diameter (see Fig. 6), the CV of the log transmission equates to the CV of the diameter (shown in Fig. 8).

Compared to SEM, the benefit of this method is in the extent of the statistics one can acquire, where arrays of several hundreds of ZMWs can be captured in a single picture and compared to each other. As an example, the corresponding CV is plotted in Fig. 8(c) as a function of diameter. This information corroborates the conclusion provided by the SEM data pertaining to the uniformity of the arrays produced (see Fig. 7).

Applications

To confirm that optical confinement was achieved for these fabricated ZMWs, we performed FCS. The focal volume was measured as a function of ZMW diameter for Alexa488 dye. The raw data are shown in Fig. 9(a). As diameter increases, the normalized FCS curves shift progressively to the right, indicating that the residence time progressively increases. This trend is not due to the change in lateral con-

finement linked to the diameter change, but entirely due to the change in the vertical rate of decay of intensity and collection efficiency in the ZMW.[16,30] In effect, this is because fluorescence correlation spectroscopy is sensitive only to diffusion displacements that move the fluorophore in or out of the detection area. Only moves that yield a change in the detectability of the fluorophore have an impact on FCS measurements.

The rate of light decay in the ZMW is a strong function of the diameter. By fitting the individual FCS curves to an appropriate FCS model,[30] the diffusion time τ_D can be calculated. From τ_D, the decay length L ($\tau_D = L^2/D$ where D is the diffusion constant of the fluorophore, 2.6×10^{-6} cm^2/s in the case of Alexa488) can be calculated, and compared to the diameter of the structures as determined by SEM [Fig. 9(b)].

Similarly, the total confinement in the ZMW can be studied by extrapolating the ordinate of the FCS curve at the origin. The reciprocal of $G(0)$ is, in the assumption of a low background noise, a measure of the occupation number N, i.e., the average number of fluorophores in the focal volume. As the diameter decreases, N will decrease as well [Fig. 9(c)]. At 10 μM concentration, less than one molecule is present on average in the focal volume of ZMWs whose diameter is below 80 nm. At 20 μM concentration, ZMWs having diameters below 65 nm still show single fluorophore occupancy.

CONCLUSION

In summary, it has been shown that ZMW structures can be manufactured in large quantities using a negative tone process using either electron beam lithography or DUV photolithography. While previous manufacturing techniques suffered from either lack of uniformity or low throughput, the NEMS process yields acceptable uniformity while maintaining a high throughput. The structures have been characterized using a variety of analytical techniques, including SEM, TEM, and optical microscopy to demonstrate the quality, controllability, and robustness of the NEMS process. Measurement of free-dye diffusion by fluorescence correlation spectroscopy illustrated the performance of ZMWs fabricated by the NEMS process. The structures show excellent confinement, which allows for single-molecule detection at concentrations of up to 20 μM. Finally, the demonstrated use of a DUV stepper for producing features in the desired size range shows that a full HVM solution at wafer scale is feasible. This assures that ZMW chips could be manufactured in quantities similar to those routinely produced in CMOS foundries.

ACKNOWLEDGMENTS

The authors would like to thank J. Puglisi for comments on the manuscript and A. Talebi for his advice on statistical analysis and methods.

[1] M. Eigen and R. Rigler, Proc. Natl. Acad. Sci. U.S.A. **91**, 5740 (1994).
[2] E. A. Lipman, B. Schuler, O. Bakajin, and W. A. Eaton, Science **301**, 1233 (2003).
[3] X. Zhuang, L. E. Bartley, H. P. Babcock, R. Russell, T. Ha, D. Herschlag, and S. Chu, Science **288**, 2048 (2000).
[4] X. S. Xie, J. Chem. Phys. **117**, 11024 (2002).
[5] D. Magde, W. W. Webb, and E. Elson, Phys. Rev. Lett. **29**, 705 (1972).
[6] T. A. Klar, S. Jakobs, M. Dyba, A. Egner, and S. W. Hell, Proc. Natl. Acad. Sci. U.S.A. **97**, 8206 (2000).
[7] K. Svoboda, C. F. Schmidt, B. J. Schnapp, and S. M. Block, Nature (London) **365**, 721 (1993).
[8] J. T. Mannion and H. G. Craighead, Biopolymers **85**, 131 (2007).
[9] M. Foquet, J. Korlach, W. Zipfel, W. W. Webb, and H. G. Craighead, Anal. Chem. **74**, 1415 (2002).
[10] M. Foquet, J. Korlach, W. R. Zipfel, W. W. Webb, and H. G. Craighead, Anal. Chem. **76**, 1618 (2004).
[11] S. M. Stavis, J. B. Edel, K. T. Samiee, and H. G. Craighead, Biophys. J. **88**, 163A (2005).
[12] S. M. Stavis, J. B. Edel, Y. Li, K. T. Samiee, D. Luo, and H. G. Craighead, J. Appl. Phys. **98**, 044903 (2005).
[13] S. M. Stavis, J. B. Edel, Y. G. Li, K. T. Samiee, D. Luo, and H. G. Craighead, Nanotechnology **16**, S314 (2005).
[14] W. E. Moerner and W. P. Ambrose, Phys. Rev. Lett. **66**, 1376 (1991).
[15] L. Kador, D. E. Horne, and W. E. Moerner, J. Phys. Chem. **94**, 1237 (1990).
[16] H. J. Levene, J. Korlach, S. W. Turner, M. Foquet, H. G. Craighead, and W. W. Webb, Science **299**, 682 (2003).
[17] A. Kramer, W. Trabesinger, B. Hecht, and U. P. Wild, Appl. Phys. Lett. **80**, 1652 (2002).
[18] E. Popov, M. Neviere, J. Wenger, P.-F. Lenne, H. Rigneault, P. Chaumet, N. Bonod, J. Dintinger, and T. Ebbesen, J. Opt. Soc. Am. A **23**, 2342 (2006).
[19] R. C. Dunn, Chem. Rev. (Washington, D.C.) **99**, 2891 (1999).
[20] Y. D. Liu and S. Blair, Opt. Lett. **28**, 507 (2003).
[21] J. Enderlein, Biophys. J. **80**, 149A (2001).
[22] T. Liebermann and W. Knoll, Colloids Surf., A **171**, 115 (2000).
[23] E. J. Sanchez, L. Novotny, and X. S. Xie, Phys. Rev. Lett. **82**, 4014 (1999).
[24] R. C. Dunn, G. R. Holtom, L. Mets, and X. S. Xie, J. Phys. Chem. **98**, 3094 (1994).
[25] X. S. Xie and R. C. Dunn, Science **265**, 361 (1994).
[26] G. I. Mashanov, D. Tacon, A. E. Knight, M. Peckham, and J. E. Molloy, Methods **29**, 142 (2003).
[27] N. L. Thompson, T. P. Burghardt, and D. Axelrod, Biophys. J. **33**, 435 (1981).
[28] B. Lu, C. L. Lu, and Y. Wei, Anal. Lett. **25**, 1 (1992).
[29] X. H. Fang and W. H. Tan, Anal. Chem. **71**, 3101 (1999).
[30] K. T. Samiee, M. Foquet, L. Guo, E. C. Cox, and H. G. Craighead, Biophys. J. **88**, 2145 (2005).
[31] K. T. Samiee, J. M. Moran-Mirabal, Y. K. Cheung, and H. G. Craighead, Biophys. J. **90**, 3288 (2006).
[32] J. B. Edel, M. Wu, B. Baird, and H. G. Craighead, Biophys. J. **88**, L43 (2005).
[33] R. C. Dunn, E. V. Allen, S. A. Joyce, G. A. Anderson, and X. S. Xie, Ultramicroscopy **57**, 113–117 (1995).
[34] A. Degiron, H. J. Lezec, W. L. Barnes, and T. W. Ebbesen, Appl. Phys. Lett. **81**, 43279 (2002).
[35] R. C. Gonzalez and R. E. Woods, *Digital Image Processing* (Prentice Hall, Upper Saddle River, N. J. 2002)..
[36] S. A. Campbell, *The Science and Engineering of Microelectronic Fabrication* (Oxford University Press, Oxford, New York, 1996)..
[37] H. A. Bethe, Phys. Rev. **66**, 163 (1944).
[38] C. J. Bouwkamp, "On Bethe's theory of diffraction by small holes," Report No. 5, 1950.
[39] F. de Abajo, Opt. Express **10**, 1475 (2002).
[40] A. Roberts, J. Opt. Soc. Am. A **4**, 1970 (1987).